

The Role of Phase Space in Complex Fragment Emission from Low to Intermediate Energies

L.G. Moretto, R. Ghetti, K. Jing, L. Phair, K. Tso, G.J. Wozniak

Nuclear Science Division

Lawrence Berkeley National Laboratory, Berkeley, CA 94720

ABSTRACT

The experimental emission probabilities of complex fragments by low energy compound nuclei and their dependence upon energy and Z value are compared to the transition state rates. Intermediate-mass-fragment multiplicity distributions for a variety of reactions at intermediate energies are shown to be binomial and thus reducible at all measured transverse energies. From these distributions a single binary event probability can be extracted which has a thermal dependence. A strong thermal signature is also found in the charge distributions. The n -fold charge distributions are reducible to the 1-fold charge distributions through a simple scaling dictated by fold number and charge conservation.

1. Transition State Rates and Complex Fragment Decay Widths

The rates for fission decay, as well as for chemical reactions, are calculated most often by means of the transition state method [1]. In this approach, the reaction rate is equated to the flux of phase space density across a “suitably” located hyperplane normal to the “reaction coordinate”. The “suitable” location is typically chosen at a saddle point in collective coordinate space, which corresponds to a bottleneck in phase space. A smart choice of the transition state location should minimize the number of phase space trajectories doubling back across the hyperplane.

The surprising success of the transition state method has prompted attempts to justify its validity in a more fundamental way, and to identify regimes in which deviations might be expected [2, 3, 4]. In what follows we shall compare experimental decay rates for complex fragment emission with transition state predictions, and search for energy E and atomic number Z dependent deviations that can be expected to exist.

The transition state expression for the fission decay width is:

$$\Gamma_f = \frac{1}{2\pi\rho(E)} \int \rho^*(E - B_f - \epsilon) d\epsilon \approx \frac{T_f \rho^*(E - B_f)}{2\pi \rho(E)}, \quad (1)$$

where $\rho(E)$ is the level density of the compound nucleus, $\rho^*(E - B_f - \epsilon)$ is the level density at the saddle point, B_f is the fission barrier, ϵ is the kinetic energy over the saddle along the fission coordinate and

$$\frac{1}{T_f} = \left. \frac{\partial [\ln \rho^*(x)]}{\partial x} \right|_{E-B_f}. \quad (2)$$

For the one dimensional case in which the only degree of freedom treated explicitly is the reaction coordinate, the decay width takes the form:

$$\Gamma_f = \hbar\omega \frac{\rho^*(E - B_f)}{\rho^*(E)} \approx \hbar\omega e^{-B_f/T}, \quad (3)$$

where T is the temperature of the transition state. Now both level densities correspond to the same number of degrees of freedom. The quantity $\hbar\omega$ is the oscillator phonon associated with the ground state minimum.

The emission of complex fragments can be treated in an analogous fashion by introducing the ridge line of conditional saddle points [5]. Each mass or charge emission can be associated with a conditional barrier. These barriers can be measured with techniques similar to those used to determine fission barriers [6]. Recently, nearly complete ridge lines have been determined for several nuclei: ^{75}Br [7], $^{90,94}\text{Mo}$ [8], and $^{110,112}\text{In}$ [6].

The emission rate of a fragment of a given mass or charge can still be described by an expression similar to that of Eq. (3). The quantity B_f becomes the conditional barrier B_Z ; but what is now the meaning of $\hbar\omega$? Is there a single value of $\hbar\omega$ for all the channels or has each channel its own characteristic frequency? We shall endeavor to answer this question experimentally.

An additional aspect of the problem has been studied by Kramers in his seminal work [2]. Kramers considered the diffusion of the system from the reactants' region to the products' region from the point of view of the Fokker-Planck equation. The new parameter entering the problem is the viscosity coefficient, which couples the reaction coordinate to the heat bath. The stationary current solution found by Kramers leads to expressions for the reaction rates similar to that of the transition state theory, differing only in the pre-exponential factor, which now includes the viscosity. More recent work on the same equation has shown that if the system is forced to start at time $t=0$ at the ground state minimum, a transient time τ_f exists during which the reaction rate goes from zero to its stationary value [3]. Both effects would decrease the overall fission rate compared to the transition state prediction.

These effects have been advocated as an explanation for the large number of precission neutrons observed in the fission of many systems [9, 10, 11, 12, 13], in apparent contradiction with the predictions of the transition state method [11, 12]. The precission neutrons can be emitted either before the system reaches the saddle point, or during the descent from saddle to scission. Only the former component,

however, has any bearing on possible deviations of the fission rate from its transition state value, and the separation of the two components is very difficult indeed.

Furthermore, it has been suggested that the viscosity and the transient time may depend on the collectivity of the reaction coordinate [14]. More specifically, the reaction coordinate for a very asymmetric decay should have little collectivity, while that for a symmetric decay should be very collective. A study of precession particles as a function of the size of the emitted fragment claims to have observed such an effect [11, 14, 15].

We are going to show that the presence or absence of the effects discussed above can be directly observable in the excitation functions for the emission of fragments with different Z values. Our procedure uses the transition state prediction as a null hypothesis, and involves only the replottting of experimental data without using any specific model. The cross section for the emission of a fragment of a given Z value can be written as:

$$\sigma_Z = \sigma_0 \frac{\Gamma_Z}{\Gamma_T} = \sigma_0 \frac{\Gamma_Z}{\Gamma_n + \Gamma_p + \dots}, \quad (4)$$

where σ_0 is the compound nucleus formation cross section and Γ_T , Γ_n , Γ_p , Γ_Z are the total-, neutron-, proton-, and Z -decay widths, respectively. Notice that Γ_T is essentially independent of Z if we confine our observations to the excitation energy region where the complex fragment emission probability is small.

We now rewrite Eq. (4) as follows:

$$\frac{\sigma_Z}{\sigma_0} \Gamma_T \frac{2\pi\rho(E - E_r^{gs})}{T_Z} = \rho(E - B_Z - E_{r,Z}^s), \quad (5)$$

where T_Z is the temperature at the conditional saddle point and E_r^{gs} , $E_{r,Z}^s$ are the ground state and saddle point rotational energies. In this way, the left hand side of the equation contains the complex fragment cross section which can be measured, and other calculable quantities that do not depend on Z , except T_Z which is only weakly dependent on Z . The right hand side contains only the level density at the conditional saddle calculated at the intrinsic excitation energy over the conditional saddle, which is calculable if the barrier height is known.

By using the standard Fermi gas level density expression, one can rewrite Eq. (5) in the following way which takes out the A -dependence of the level density:

$$\frac{\ln \left[\frac{\sigma_Z}{\sigma_0} \Gamma_T \frac{2\pi\rho(E - E_r^{gs})}{T_Z} \right]}{2\sqrt{a_n}} = \frac{\ln R_f}{2\sqrt{a_n}} = \sqrt{\frac{a_Z}{a_n}} (E - B_Z - E_r^s), \quad (6)$$

where a_Z , a_n are the saddle and ground state level density parameters. A plot of the left hand side of this equation versus the square root of the intrinsic excitation energy over the saddle should give a straight line, and the slope of this straight line should give the square root of a_Z/a_n .

Recently, the excitation functions for a large number of fragment Z values have been measured for the following systems: ^{75}Br [7], $^{90,94}\text{Mo}$ [8], and $^{110,112}\text{In}$ [6]. The

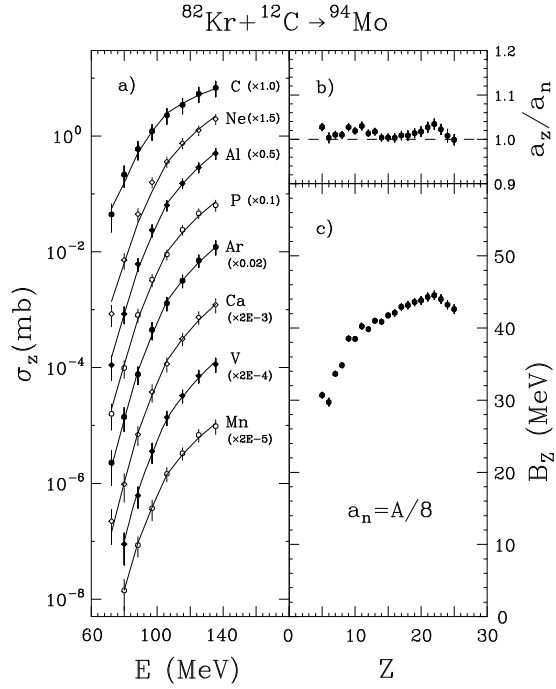


Fig. 1: a) The excitation functions (cross sections vs excitation energy) for complex fragments of some typical Z values emitted from the compound nucleus ^{94}Mo produced in the reaction $^{82}\text{Kr} + ^{12}\text{C}$ at beam energies ranging from 6.2 to 12.2 MeV/u. b) The a_z/a_n values and c) conditional barriers B_z , both extracted by fitting the excitation functions with a transition state formalism. The solid lines in a) correspond to the fit using an energy level parameter $a_n = A/8$.

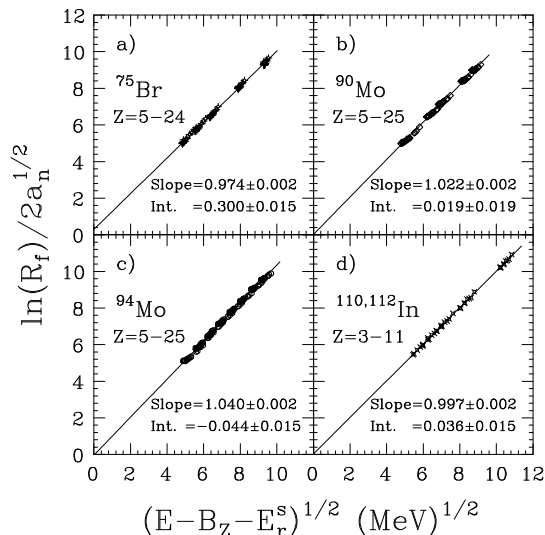


Fig. 2: $\ln R_f/2\sqrt{a_n}$ (see Eq. (6) and text) vs the square root of the intrinsic excitation energy for four compound nuclei: ^{75}Br a), ^{90}Mo b), ^{94}Mo c), and $^{110,112}\text{In}$ d). All the excitation functions for the indicated Z range are included for each compound nucleus. The solid lines are the linear fits to the data. The error bars are smaller than the size of symbols.

corresponding conditional barriers have been extracted by fitting the excitation functions with the transition state formalism. A level density parameter $a_n = A/8$ was assumed in the fitting. As an example, Fig. 1a shows some of the excitation functions for fragments with Z -values from 5 to 25 for the compound nucleus ^{94}Mo . The solid lines in Fig. 1a correspond to the best fit to the experimental data. The extracted ratios a_Z/a_n are close to unity for all Z values (see Fig. 1b). The extracted conditional barriers increase from 30-45 MeV as the charge of the emitted fragment increases (see Fig. 1c).

Eq. (6) suggests that it should be possible to reduce *all* the excitation functions for the emission of different complex fragments from a given system to a single straight line. In Fig. 2 all the excitation functions associated with each of four compound nuclei (^{75}Br , ^{90}Mo , ^{94}Mo , and $^{110,112}\text{In}$) are plotted according to Eq. (6). There are 20, 21, 21, and 9 excitation functions for ^{75}Br , ^{90}Mo , ^{94}Mo , and $^{110,112}\text{In}$, respectively. We see that all the excitation functions for each Z -value fall with remarkable precision on the same line that is in fact straight, has a slope near unity and passes closely through zero.

As a final virtuoso touch, we can try to collapse ALL the excitation functions for ALL Z values and for all compound nuclei into a single straight line. The resulting plot for four different compound nuclei is shown in Fig. 3. It includes a total of 71 excitation functions spanning a Z range from 3 to 25. The collapse of all the experimental excitation functions for all of the different Z -values and all the systems onto a single straight line is strong evidence for the validity of the transition state formalism and for the absence of Z - and E -dependent deviations. In particular, one is

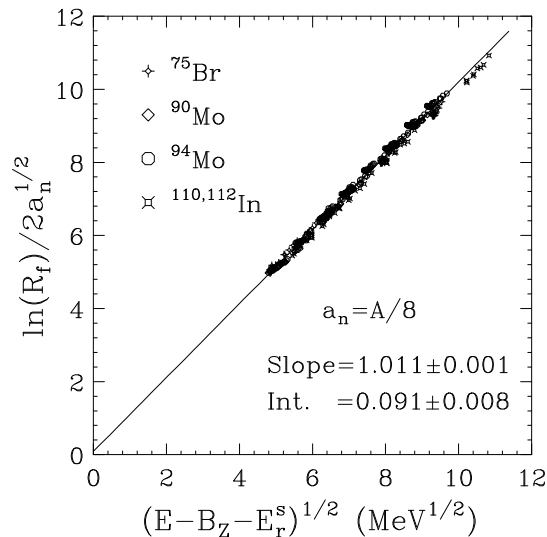


Fig. 3: The same as Fig. 2 with data for all four nuclei in a single plot. The straight line is the linear fit to all the data points.

led to the following conclusions: a) Once one removes the phase space associated with the non reactive degrees of freedom at the conditional saddle point, the reduced rates are IDENTICAL for fragments of all Z -values. Within the experimental sensitivity, the quantity $\hbar\omega$ in Eq. (2) appears to be Z independent. b) For all fragments, there is no deviation from the expected linear dependence over the excitation energy range from 50-130 MeV explored. This seems to rule out, for all Z -values, transient time effects which should become noticeable with increasing excitation energy. c) The slope, which corresponds to the $\sqrt{a_Z/a_n}$, is essentially 1 for all Z values of all systems studied. d) The intercept of the straight line, which is associated with the channel frequency ω , is essentially zero and shows no obvious dependence on the fragment Z -values (i.e., the collectivity).

We conclude that in this extended data set there is no evidence for transient effects either directly or through their expected dependence upon the mass of the emitted fragment. Furthermore it appears that the channel frequency is the same for all the different Z decay channels.

2. Reducibility at intermediate energies

At low excitation energies, complex fragments are emitted with low probability by a compound nucleus mechanism [16, 17]. At increasingly larger energies, the probability of complex fragment emission increases dramatically, until several fragments are observed within a single event [18, 19, 20]. The nature of this multifragmentation process is at the center of much current attention. For example, the timescale of fragment emission and the associated issue of sequentiality versus simultaneity are the objects of intense theoretical and experimental study.

Recent experimental work [21, 22] has shown that the excitation functions for the production of two, three, four, etc. fragments give a characteristically linear Arrhenius plot, suggesting a statistical energy dependence.

A fundamental issue, connected in part to those mentioned above, is that of reducibility: can multifragmentation be reduced to a combination of (nearly) independent emissions of fragments? More to the point, can the probability for the emission of n fragments be reduced to the emission probability of just one fragment?

Recently, it has been experimentally observed in many reactions that for any value of the transverse energy E_t , the n -fragment emission probability P_n is reducible to the one-fragment emission probability p through a binomial distribution [23, 24]

$$P_n^m = \frac{m!}{n!(m-n)!} p^n (1-p)^{m-n}. \quad (7)$$

This empirical evidence indicates that multifragmentation can be thought of as a special combination of nearly independent fragment emissions. The binomial combination of the elementary probabilities points to a combinatorial structure associated with a time-like or space-like one-dimensional sequence. It was also found that the log of such one-fragment emission probabilities ($\log p$) plotted vs $1/\sqrt{E_t}$ (Arrhenius plot) gives a remarkably straight line. This linear dependence is strongly suggestive of a thermal nature for p ,

$$p = e^{-B/T} \quad (8)$$

under the assumption that the temperature $T \propto \sqrt{E^*}$ where E^* is the excitation energy. Examples of the binomial decomposition of the n -fragment emission probabilities P_n into a one-fragment emission probability p , and the resulting Arrhenius plot for p is given in Fig. 4. The extraordinary quantitative agreement between the calculations and the experimental data confirms the binomiality of the multifragmentation process.

The more directly interpretable physical parameter contained in this analysis is the binary barrier B (proportional to the slope of the Arrhenius plot in Fig. 4). One may wonder why a single binary barrier suffices, since mass asymmetries with many different barriers may be present. Let us consider a barrier distribution as a function of mass asymmetry x of the form $B = B_0 + ax^n$, where B_0 is the lowest barrier in the range considered. Then,

$$p = \frac{\Gamma}{\hbar\omega_0} = \int e^{-B_0/T} e^{-ax^n/T} dx \cong \left(\frac{T}{a}\right)^{1/n} e^{-B_0/T} \quad (9)$$

Thus the simple form of Eq. (8) is retained with a small and renormalizable pre-exponential modification.

One possible interpretation of the reducibility discussed above is sequential decay with constant probability p . Assuming that the (small) fragments, once produced

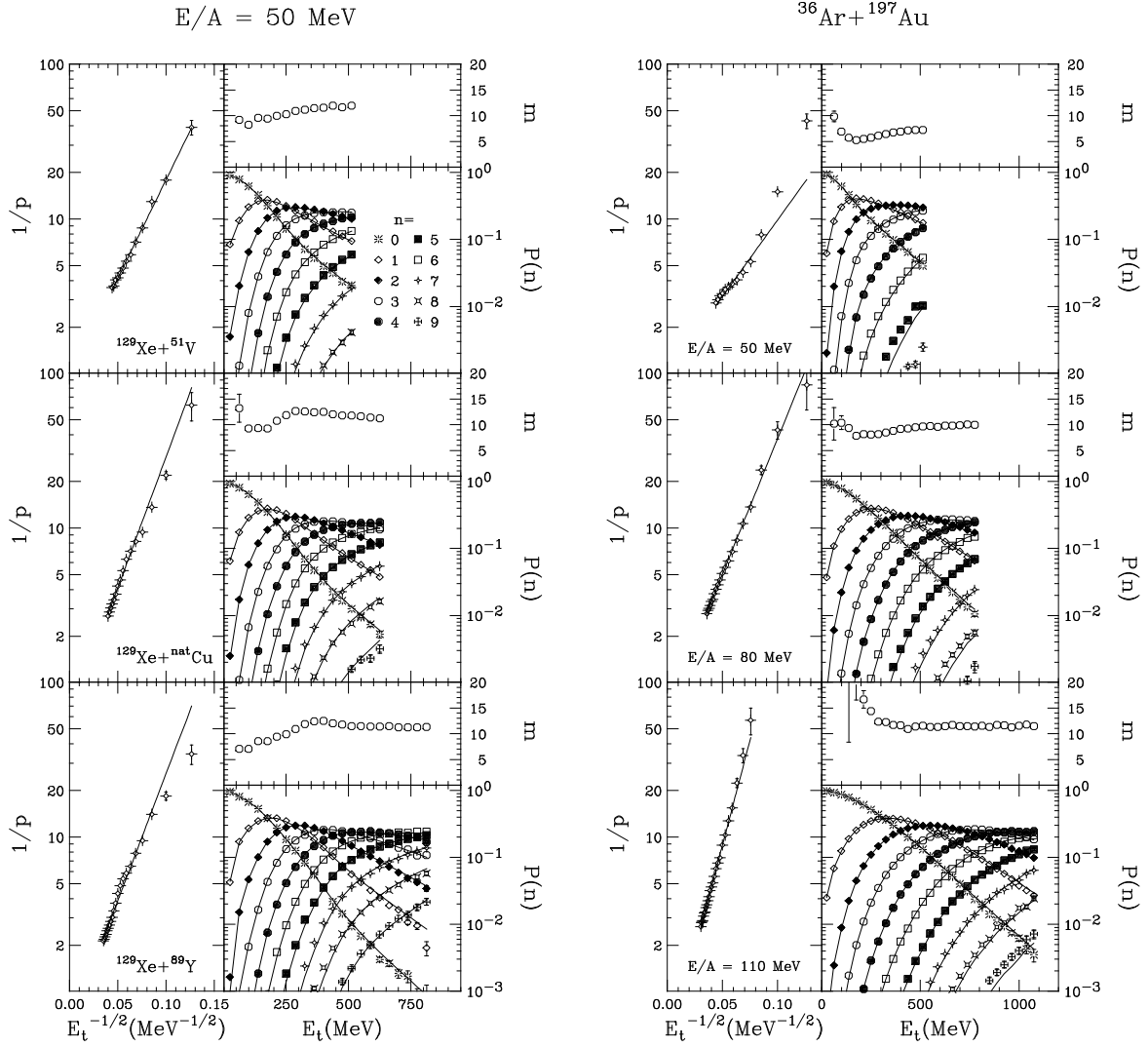


Fig. 4: For the ^{129}Xe induced reactions at $E/A=50$ MeV (left figure) and the $^{36}\text{Ar}+^{197}\text{Au}$ reactions at $E/A=50, 80$ and 110 MeV (right figure): (left panel) the reciprocal of the single fragment emission probability $1/p$ as a function of $1/\sqrt{E_t}$; and (right panel) the parameter m (number of the throws in the binomial distribution) and the probability $P(n)$ of emitting n intermediate mass fragments (IMF, $3 \leq Z \leq 20$) as a function of the transverse energy E_t . The solid lines through the excitation functions correspond to binomial distributions calculated with the given values of m and p . (See Eq. (7))

do not generate additional fragments or disappear, the binomial distribution follows directly. In this framework, it is possible to translate the probability p into the mean time separation between fragments. In other words, we can relate the n -fragment emission probabilities to the mean time separations between fragments. The validity of this interpretation is testable by experiment.

We have tried to find alternative explanations to the sequential description for the binomial distributions with thermal probabilities. An obvious model is a chain of m links with probability p that any of the links is broken. The probability that n links are broken is given by Eq. (7). This result is, of course, strictly dependent on the dimensionality of the model, and its relevance to multifragmentation is unclear. Nevertheless, it stresses again the *fundamental reducibility* of the multifragmentation probability to a binary breakup probability p .

3. Charge Distributions

These aspects of reducibility and thermal scaling in the integrated fragment emission probabilities lead naturally to the question: Is the charge distribution itself reducible and scalable? In particular, what is the charge distribution form that satisfies the condition of reducibility and of thermal dependence?

Let us first consider the aspect of reducibility as it applies to the charge distributions. In its broadest form, reducibility demands that the probability $p(Z)$, from which an event of n fragments is generated by m trials, is the same at every step of extraction. The consequence of this extreme reducibility is straightforward: the charge distribution for the one-fold events is the same as that for the n -fold events and equal to the singles distributions, i.e.:

$$P_{(1)}(Z) = P_{(n)}(Z) = P_{singles}(Z) = p(Z). \quad (10)$$

We now consider the consequences of the thermal dependence of p [23] on the charge distributions. If the one-fold = n -fold = singles distributions is thermal, then

$$P(Z) \propto e^{-\frac{B(Z)}{T}} \quad (11)$$

or $T \ln P(Z) \propto -B(Z)$. This suggests that, under the usual assumption $E_t \propto E^*$ [23], the function

$$\sqrt{E_t} \ln P(Z) = D(Z) \quad (12)$$

should be independent of E_t .

In the $^{36}\text{Ar}+^{197}\text{Au}$ reaction, as in other reactions [25, 26], the IMF charge distributions are empirically found to be nearly exponential functions of Z

$$P_n(Z) \propto e^{-\alpha_n Z}. \quad (13)$$

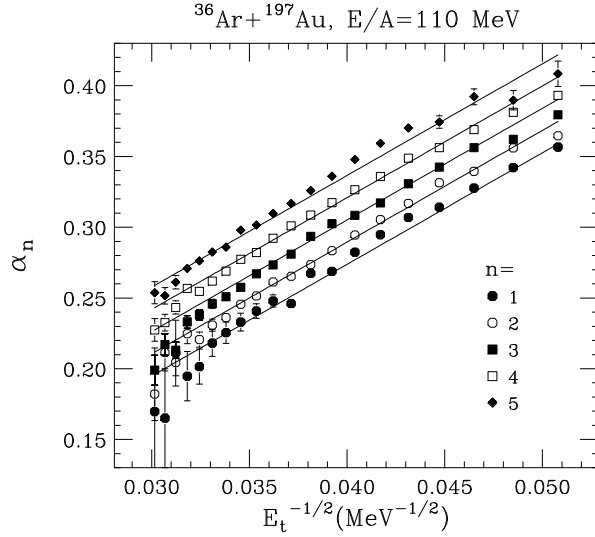


Fig. 5: The exponential fit parameter α_n (from fits to the charge distributions, see Eq.(13)) is plotted as a function of $1/\sqrt{E_t}$. The solid lines are a fit to the values of α_n using Eq. (15).

In light of the above considerations, we would expect for α_n the following simple dependence

$$\alpha_n \propto \frac{1}{T} \propto \frac{1}{\sqrt{E_t}} \quad (14)$$

for all folds n . Thus a plot of α_n vs $1/\sqrt{E_t}$ should give nearly straight lines. This is shown in Fig. 5 for $^{36}\text{Ar}+^{197}\text{Au}$ at $E/A=110$ MeV.

The expectation of thermal scaling appears to be met quite satisfactorily. For each value of n the exponent α_n shows the linear dependence on $1/\sqrt{E_t}$ anticipated in Eq. (14). On the other hand, the extreme reducibility condition demanded by Eq. (10), namely that $\alpha_1 = \alpha_2 = \dots = \alpha_n = \alpha$, is not rigorously met. Rather than collapsing on a single straight line, the values of α_n for the different fragment multiplicities are offset one with respect to another by what appears to be a small constant quantity.

In fact, one can fit all of the data remarkably well, assuming for α_n the form:

$$\alpha_n = \frac{K'}{\sqrt{E_t}} + nc \quad (15)$$

which implies:

$$\alpha_n = \frac{K}{T} + nc \quad (16)$$

or more generally, for the Z distribution:

$$P_n(Z) \propto e^{-\frac{B(Z)}{T} - ncZ}. \quad (17)$$

Thus, we expect a more general reducibility expression for the charge distribution of any form to be:

$$[\ln P_n(Z) + ncZ] \sqrt{E_t} = F(Z) \quad (18)$$

for all values of n and E_t . This equation indicates that it should be possible to reduce the charge distributions associated with any intermediate mass fragment multiplicity to the charge distribution of the singles.

What is the origin of the regular offset that separates the curves in Fig. 5? The general form of Eq. (17) suggests the presence of an entropy term that does not depend explicitly on temperature. The general expression for the free energy (in terms of enthalpy H , temperature T and entropy S)

$$\Delta G = \Delta H(Z) - T\Delta S(Z) \quad (19)$$

leads to the distribution

$$P(Z) \propto e^{-\frac{\Delta H(Z)}{T} + \Delta S}. \quad (20)$$

Typically, ΔS is of topological or combinatorial origin. For instance, a factor of this sort would appear in the isomerization of a molecule involving a change of symmetry. In our specific case ΔS may point to an asymptotic combinatorial structure of the multifragmentation process in the high temperature limit. As an example, we consider the Euler problem of an integer to be written as the sum of smaller integers, and calculate the resulting integer distribution. Specifically, let us consider an integer Z_0 to be broken into n pieces. Let n_Z be the number of pieces of size Z . It can be shown [27] that

$$n_Z = \frac{n^2}{Z_0} e^{-\frac{nZ}{Z_0}} = cn^2 e^{-cnZ}. \quad (21)$$

This expression has the correct asymptotic structure for $T \rightarrow \infty$ required by Eq. (17). The significance of this form is transparent: First, the overall scale for the fragment size is set by the total charge Z_0 . Second, for a specific multiplicity n , the scale is reduced by a factor n to the value Z_0/n .

4. Phase Coexistence

While Eq. (21) obviously implies charge conservation, it is not necessary that charge conservation be implemented as suggested by it. In fact it is easy to envisage a regime where the quantity c should be zero. Sequential thermal emission is a case in point. Since any fragment does not know how many other fragments will follow its emission, its charge distribution can not reflect the requirement of an unbiased partition of the total charge among n fragments. We have in mind a liquid drop evaporating fragments of different size and binding energy. ‘‘Charge conservation’’ will affect the distribution minimally, unless evaporation consumes the entire system, and even then, not in the sense of an unbiased partition.

On the other hand, in a simultaneous emission controlled by a n -fragment transition state [28, 29], fragments would be strongly aware of each other, and would reflect such an awareness through the charge distribution.

The question then arises whether $c = 0$ or $c > 0$, or even better, whether one can identify a transition from a regime for which $c = 0$ to a new regime for which

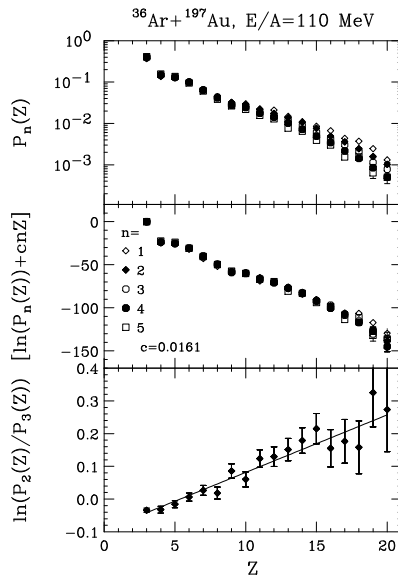


Fig. 6: Top panel: the n gated charge distributions $P_n(Z)$ for the reaction $^{36}\text{Ar}+^{197}\text{Au}$ at $E/A=110$ MeV. The charge distributions were constructed from events with $E_t=650\pm 20$ MeV and $n=1-5$. Middle panel: the “reduced” charge distribution [27] for the same data using the indicated value of c . (The data here are normalized at $Z=3$). Bottom panel: the log of the ratio of $P_2(Z)/P_3(Z)$. The slope corresponds to c for $n=2$ (see Eq.(22)). The statistical error bars are shown for errors larger than the symbol size.

$c > 0$. In order to answer this question, we have studied the charge distributions as a function of fragment multiplicity n and transverse energy E_t for a number of systems and excitation energies. Specifically, we will present data for the reaction $^{36}\text{Ar}+^{197}\text{Au}$ at $E/A=80$ and 110 MeV and the reaction $^{129}\text{Xe}+^{197}\text{Au}$ at $E/A=50$ and 60 MeV.

A general approach for measuring c , which does not depend on any specific form for the charge distribution, is to construct at each E_t the ratio

$$\frac{P_n(Z)}{P_{n+1}(Z)} = e^{cZ}. \quad (22)$$

A value of c can be extracted for each n by taking the log of this ratio and finding the slope of the resulting graph (see bottom panel of Fig. 6). A weighted average (over all IMF multiplicities n) for c can then be constructed at all E_t . Alternatively, a χ^2 can be constructed in terms of the differences in $F(Z)$ (see Eq. (18)) between any pairs of n values and minimized as a function of c . These procedures yield essentially the same results. These results are reported in Fig. 7 for the $^{129}\text{Xe}+^{197}\text{Au}$ and $^{36}\text{Ar}+^{197}\text{Au}$ reactions.

It is interesting to notice that for all reactions and bombarding energies the quantity c starts at or near zero, it increases with increasing E_t for small E_t values, and seems to saturate to a constant value at large E_t .

This behavior can be compared to that of a fluid crossing from the region of liquid-vapor coexistence to the region of overheated and unsaturated vapor. In the

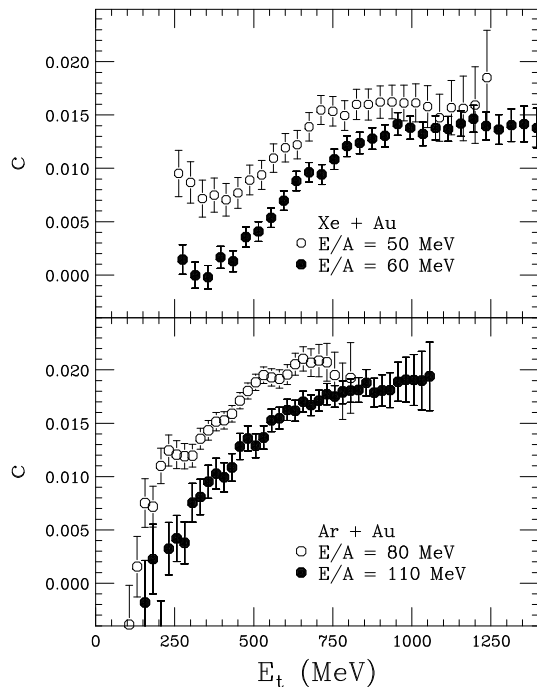


Fig. 7: Plots of the coefficient c versus E_t for the reactions $^{129}\text{Xe}+^{197}\text{Au}$ at $E/A=50$ and 60 MeV (top panel) and $^{36}\text{Ar}+^{197}\text{Au}$ at $E/A=80$ and 110 MeV (bottom panel). The error bars are statistical.

coexistence region, the properties of the saturated vapor cannot depend on the total mass of fluid. The presence of the liquid phase guarantees mass conservation at all average densities for any given temperature. A change in mean density (volume) merely changes the relative amount of the liquid and vapor, without altering the properties of the saturated vapor. Hence the vapor properties, and, in particular, the cluster size distributions cannot reflect the total mass or even the mean density of the system. In our notation, $c = 0$.

On the other hand, in the region of unsaturated vapor, there is no liquid to insure mass conservation. Thus the vapor itself must take care of this conservation, at least grand canonically. In our notation, $c > 0$.

This description should not be taken too literally, for a variety of reasons, one of which is the finiteness of the system. The $c = 0$ regime may signify an evaporative-like emission from a source which survives as a charge conserving residue (liquid), while the $c > 0$ regime may signify the complete vaporization of the source.

In order to test these ideas for a finite system, percolation calculations [30] were performed for systems of $Z_0=97$, 160 and 400 as a function of the percentage of bonds broken (p_b) in the simulation. Values of c were extracted (using Eq.(22)) as a function of p_b .

The results are shown in Fig. 8. Guided by the insight gleaned from the approximate solution to Euler's problem (see Eq.(21)) we have scaled the extracted values of

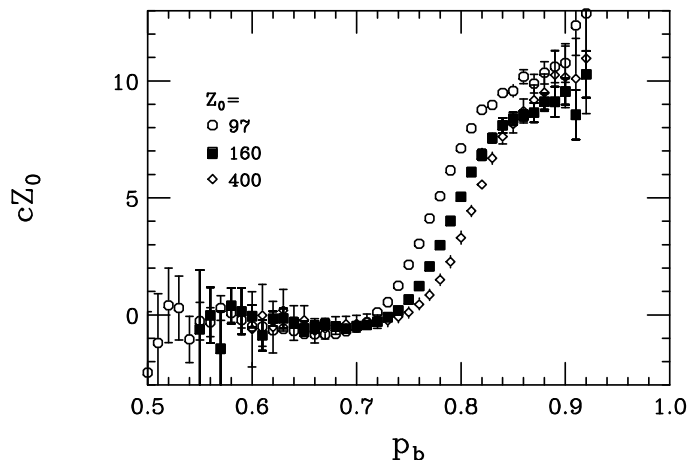


Fig. 8: A plot of cZ_0 versus the percentage of broken bonds p_b from a percolation calculation [30] for three systems $Z_0=97$ (circles), $Z_0=160$ (squares) and $Z_0=400$ (diamonds). The statistical error bars are shown for errors larger than the symbol size.

c by the source size Z_0 in order to remove this leading dependence and to evidentiate the true finite size effects. For values of p_b smaller than the critical (percolating) value ($p_b^{crit} \approx 0.75$ for an infinite system), we find $c = 0$. This is the region in which a large (percolating) cluster is present. As p_b goes above its critical value, the value of c increases, and eventually saturates in a way very similar to that observed experimentally. Due to the finiteness of the system the transition is smooth rather than sharp and can be made sharper by increasing the size of the system.

Before proceeding, let us remind ourselves that charge conservation is *not* a finite-size effect. For instance, the chemical potential, introduced in statistical mechanics to conserve mass, survives the thermodynamical limit and retains its meaning for an infinite system, despite the fact that the extensive thermodynamic quantities go to infinity. In our case, while it is true that c goes to zero or that $1/c$ goes to infinity, it is also true that the product cZ_0 tends to a finite limit nearly independent of Z_0 .

The significance of the actual experimental value of c in the region where it seems to saturate is unclear. In Eq.(21), c takes a direct meaning for the Euler problem: $c = 1/Z_0$. It should be noted that our analysis is not directly comparable to the Euler solution (Eq.(21)) since we have restricted ourselves to a limited region ($3 \leq Z \leq 20$) of the total charge distribution for our study of how the source is partitioned into different IMF multiplicities. It must also be appreciated that Eq. (21) and the associated dependence of c upon Z_0 are characteristic of a one-dimensional percolation model. In light of the points mentioned above, it is not unexpected that c appears to be proportional, but not equal, to $1/Z_0$ in the three-dimensional percolation calculation reported in Fig. 8. An interpretation of c in terms of the source size may be possible when more data and a better understanding of the percolation of finite systems are available.

Acknowledgements

This work was supported by the Director, Office of Energy Research, Office of High Energy and Nuclear Physics, Nuclear Physics Division of the US Department of Energy, under contract DE-AC03-76SF00098 and by the National Science Foundation under Grant Nos. PHY-8913815, PHY-90117077, and PHY-9214992.

5. References

- [1] E. Wigner, *Trans. Faraday Soc.* **34**, 29 (1938).
- [2] H.A. Kramers, *Physica* **7**, 284 (1940).
- [3] P. Grange *et al.*, *Phys. Rev. C* **27**, 2063 (1983).
- [4] P. Hänggi *et al.*, *Rev. Mod. Phys.* **62**, 251 (1990).
- [5] L.G. Moretto, *Nucl. Phys. A* **247**, 211 (1975).
- [6] M.A. McMahan *et al.*, *Phys. Rev. Lett.* **54**, 1995 (1985).
- [7] D.N. Delis *et al.*, *Nucl. Phys. A* **534**, 403 (1991).
- [8] L.G. Moretto *et al.*, *Phys. Rev. Lett.* **74**, 3557 (1995).
- [9] A. Gavron *et al.*, *Phys. Rev. Lett.* **47**, 1255 (1981).
- [10] E. Holub *et al.*, *Phys. Rev. C* **28**, 252 (1983).
- [11] D.J. Hinde *et al.*, *Phys. Rev. C* **45**, 1229 (1992).
- [12] D. Hilscher and H. Rossner, *Ann. Phys. Fr.* **17**, 471 (1992).
- [13] D.J. Hinde *et al.*, *Nucl. Phys. A* **452**, 550 (1986).
- [14] D. Hilscher *et al.*, *Phys. Rev. Lett.* **62**, 1099 (1989).
- [15] E. Mordhorst *et al.*, *Phys. Rev. C* **43**, 1991 (1991).
- [16] L.G. Sobotka, *et. al.*, *Phys. Rev. Lett.* **51**, 2187 (1983).
- [17] L.G. Moretto and G.J. Wozniak, *Prog. Part. & Nucl. Phys.* **21**, 401 (1988).
- [18] D. Guerreau, *Formation and Decay of Hot Nuclei: The Experimental Situation* ed. (Plenum Publishing Corp., 1989).
- [19] D.H.E. Gross, *Rep. Prog. Phys.* **53**, 605 (1990).
- [20] L.G. Moretto and G.J. Wozniak, *Ann. Rev. Part. Nucl. Sci.* **43**, 379 (1993).
- [21] L.G. Moretto, D.N. Delis, and G.J. Wozniak, *Phys. Rev. Lett.* **71**, 3935 (1993).
- [22] J. Pouliot, *et al.*, *Phys. Rev. C* **48**, 2514 (1993).
- [23] L.G. Moretto, *et al.*, *Phys. Rev. Lett.* **74**, 1530 (1995).
- [24] K. Tso *et al.*, *Phys. Lett. B* **361**, 25 (1995).
- [25] Y.D. Kim *et al.*, *Phys. Rev.* **C45**, 338 (1992).
- [26] D.R. Bowman *et al.*, *Phys. Rev.* **C46**, 1834 (1992).
- [27] L. Phair *et al.*, *Phys. Rev. Lett.* **75**, 213 (1995).
- [28] J.A. Lopez and J. Randrup, *Nucl. Phys. A* **503**, 183-222 (1989).
- [29] J.A. Lopez and J. Randrup, *Nucl. Phys. A* **512**, 345 (1990).
- [30] W. Bauer, *Phys. Rev. C* **38**, 1297 (1988).